Trap-Free Halogen Photoelimination from Mononuclear Ni(III) Complexes

Seung Jun Hwang,[†] David C. Powers,[†] Andrew G. Maher,[†] Bryce L. Anderson,[†] Ryan G. Hadt,[†] Shao-Liang Zheng,[†] Yu-Sheng Chen,[‡] and Daniel G. Nocera*,[†]

[†]Department of Chemistry and Chemical Biology, Harvard University, Cambridge, Massachusetts 02138, United States
[‡]ChemMatCARS, The University of Chicago, Argonne, Illinois 60439, United States

Ⓢ *Supporting Information*

ABSTRACT: Halogen photoelimination reactions constitute the oxidative half-reaction of closed HX-splitting energy storage cycles. Here, we report high-yielding, endothermic Cl_2 photoelimination chemistry from mononuclear Ni(III) complexes. On the basis of time-resolved spectroscopy and steady-state photocrystallography experiments, a mechanism involving ligand-assisted halogen elimination is proposed. Employing ancillary ligands to promote elimination offers a strategy to circumvent the inherently short-lived excited states of 3d metal complexes for the activation of thermodynamically challenging bonds.

Photodriven HX-splitting (X = Cl, Br, and OH) reactions underpin chemical strategies for solar-to-fuels energy conversion.[1−3] In closed, carbon-neutral HX-splitting cycles, both proton reduction and anion oxidation half-reactions must be accomplished. Despite substantial work toward halogen elimination photoreactions with 4d and 5d metal complexes, such as Pt,[4−8] Au,[9] Rh,[10] Ir, and related heterobimetallics,[11−13] halide oxidation remains the kinetic bottleneck for the majority of developed HX-splitting photocycles.[14,15] In many cases, chemical traps are required to promote halogen extrusion, which inevitably mitigates the utility of these reactions in energy-storing catalysis. Although trap-free halogen eliminations have begun to be developed,[4,6,9] little progress has been made toward energy-storing halogen elimination chemistry with earth-abundant 3d metal complexes. Here, we report a family of mononuclear Ni(III) complexes that participate in trap-free X_2 elimination photoreactions. Both time-resolved spectroscopy and steady-state photocrystallography have established critical ligand-to-chlorine-atom charge-transfer intermediates in the observed photoreactions.

The dearth of photoeliminations from 3d metal complexes is a reflection of the intrinsically short excited-state lifetimes of these complexes.[16−18] Whereas long-lived charge-transfer excited states are frequently encountered in the photochemistry of 4d and 5d transition-metal complexes, 3d transition-metal complexes typically possess extremely short-lived charge-transfer states. These short lifetimes are a consequence of the relatively small crystal field splitting, which results in low-energy ligand-field excited states that provide a mechanism for rapid nonradiative relaxation.[17,18] Strategies to overcome the short lifetimes of 3d complexes include photoredox chemistry, in which the chromophore and catalyst are decoupled,[19,20] and

ligand design strategies aimed at destabilizing low-lying ligand-field states and thus removing nonradiative pathways for rapid excited-state relaxation.[21] We report an energy-storing, photo-induced halogen elimination reaction from molecular Ni(III) complexes that utilizes a new strategy based on secondary coordination sphere effects to overcome the challenges of 3d photochemistry. Nanosecond-resolved transient absorption spectroscopy, steady-state photocrystallography, and computational methods have allowed for the observation and characterization of the M−X bond activation process.

Ni(III) trichloride complex $NiCl_3$(dppe) (**1a**) (dppe = bis(diphenylphosphino)ethane) has been prepared by treating $NiCl_2$(dppe) (**2a**) with 0.5 equiv of $PhICl_2$, as previously described.[22] Complex **1a** displays no resonances in the ^1H NMR or $\{^1H\}^{31}P$ NMR spectrum. The solid-state structure of complex **1a** was evaluated using its bromide congener $NiBr_3$(dppe) (**1b**) because diffraction-quality crystals of **1a** were not accessible. The structure of complex **1b** is illustrated in Figure 1 and features a distorted square pyramidal geometry; the basal Ni(III)−Br bonds (2.351(1) and 2.374(1) Å) are shorter than the apical Ni(III)−Br bond (2.400(1) Å). Evans method and variable-
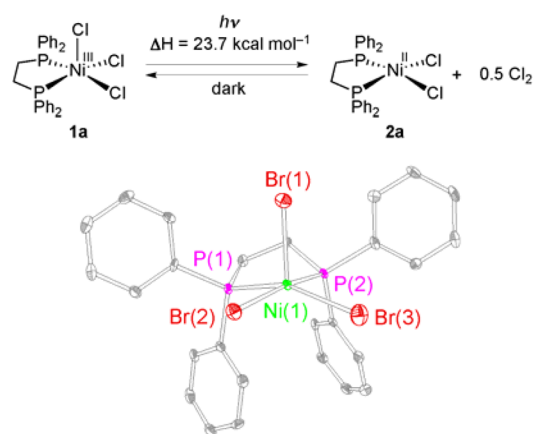

Figure 1. Photolysis of **1a** affords **2a** and Cl_2. Endothermic energy shown for the overall transformation from **1a** to **2a** was determined from calorimetry measurements. Thermal ellipsoid plot (50% probability) of representative Ni(III) trihalide complex $NiBr_3$(dppe) (**1b**) with solvent molecules and H atoms removed for clarity.

temperature EPR indicated the complexes are $S = {}^{1}/_{2}$, as expected for a mononuclear d^7 complex (Figure S1). The EPR spectra display pseudoaxial signals with $g_x = 2.245$, $g_y = 2.164$ and $g_z = 2.012$ and a four-line superhyperfine coupling pattern in the g_z direction. The superhyperfine coupling is a direct probe of the coupling of the $3d_{z^2}$ unpaired electron with the nuclear magnetic moment of the apical halide ligand ($I = {}^{3}/_{2}$ for Cl), and the magnitude is a measure of the degree of electron delocalization of the unpaired electron along the apical Ni(III)−X bond.[23]

The absorption spectrum of **1a**, given in Figure 2, exhibits two prominent bands, which are assigned to ligand-to-metal charge-
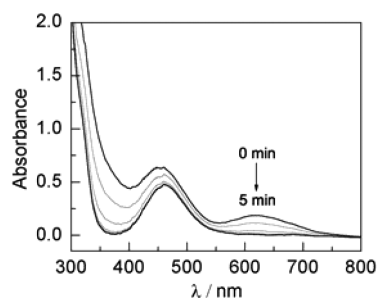

Figure 2. Photolysis of a 0.2 mM solution of **1a** in CH$_3$CN ($\lambda > 430$ nm) at 25 °C.

transfer (LMCT) transitions on the basis of time-dependent density functional theory (TD-DFT) calculations (vide infra). Steady-state photolysis of a CH$_3$CN solution of **1a** with visible light ($\lambda > 430$ nm) led to the rapid evolution of low-spin Ni(II) complex **2a**, as established by UV−vis (Figures 2 and S3) and both ^{1}H and ^{31}P NMR spectra (Figures S4 and S5, respectively). No side products were observed, and similar photochemistry also proceeded in CH$_2$Cl$_2$. Integration of the ^{1}H NMR spectrum against 1,2-dimethoxyethane as an external standard indicated that **2a** was observed in 80% yield. No olefinic traps were required to promote halogen elimination. Cl-based products of solution-phase photolysis were not characterized; photogenerated Cl radicals are expected to participate in H atom abstraction reactions with either CH$_3$CN[24,25] or CH$_2$Cl$_2$.[26] Wavelength-dependent quantum yields for halogen elimination from **1a** were measured in CH$_3$CN against a potassium ferrioxalate standard actinometer and were determined to be 77% (370 nm), 76% (434 nm), and 9% (510 nm). These data are consistent with a common, productive excited state that is accessed upon 370 and 434 nm irradiation,[27] indicating rapid internal conversion to a lower-energy, photodissociative state. The substantially lower quantum yield at 510 nm indicates that the higher-energy LMCT transition ($\lambda_{max} \approx 450$ nm) is responsible for efficient halogen photoelimination.

Solid-state irradiation of **1a** ($\sim$20 Torr, 25 °C, $\lambda > 350$ nm) results in the formation of **2a** (87% yield on the basis of recovered starting material determined by ^{1}H NMR versus external standard 1,2-dimethoxyethane; Figure S6) with concurrent evolution of half an equivalent of Cl$_2$. Evolved Cl$_2$ was collected at 77 K and subsequently characterized by mass spectrometric analysis of gaseous reaction products: m/z corresponding to ^{35,35}Cl$_2$, ^{37,37}Cl$_2$, ^{35,37}Cl$_2$, ^{35}Cl·, and ^{37}Cl· were observed, and the measured ratio of ^{35}Cl and ^{37}Cl was in good agreement with the natural isotopic abundance for chlorine (Figure 3).[28] The yield of evolved Cl$_2$ (82%) was quantified colorimetrically by trapping evolved halogen with N,N-diethyl-1,4-phenylenediamine sulfate (DPD) to afford the intensely pink radical cation DPD$^{•+}$ (Figure
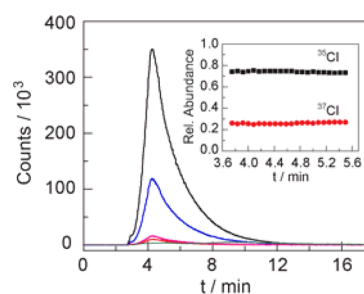

Figure 3. Mass spectrometry analysis of the gas evolved from solid-state photolysis of complex **1a**. Traces correspond to ^{35}Cl (black), ^{37}Cl (blue), ^{35}Cl^{35}Cl (pink), ^{35}Cl^{37}Cl (red), and ^{37}Cl^{37}Cl (green) mass fragments. Inset: relative abundance of ^{35}Cl (black) and ^{37}Cl (red).

S7).[29,30] No reduction of **1a** was observed by ^{1}H NMR, ^{31}P NMR, or UV−vis spectroscopy after heating a powdered sample of **1a** at 70 °C in the exclusion of light and moisture, confirming that halogen elimination is photochemically, and not thermally, driven (Figure S8).

The energy-storage capacity of Cl$_2$ photoelimination from **1a** was established by solution calorimetric measurements of chlorine addition to **2a** to afford **1a** (i.e., the reverse of halogen elimination). Using the known heat of reaction of PhICl$_2$ → PhI + Cl$_2$,[31] ΔH for Cl$_2$ extrusion from **1a** was determined to be +23.7 kcal mol^{-1} (Figure S9). DFT calculations at the B3LYP level of theory with the SDD basis set for Ni, P, and Br and 6-311++G** for all other atoms are consistent with our experimental values (Table S8). Computationally, the elimination of Cl$_2$ from **1a** is +20.3 and +13.4 kcal mol^{-1} for ΔH and ΔG, respectively. The energy stored in Cl$_2$ elimination from **1a** is similar to the most endothermic halogen elimination reactions that have been achieved with noble metal complexes.[7]

Nanosecond-resolved transient absorption (TA) spectroscopy was used to investigate the mechanism of Cl$_2$ photoelimination from **1a** in solution. Figure S10 shows the time evolution of the TA spectrum obtained from laser flash photolysis (355 nm pump) of a CH$_3$CN solution of **1a**. The prompt TA spectrum observed at 40 ns evolves over the course of several microseconds into a spectrum that corresponds to that of the formation of **2a** from **1a**; single-wavelength kinetics were monitored at 540 nm and provided a lifetime for the TA signal of 3.43 $\pm$ 0.05 μs. The initial 40 ns spectrum is accounted for by the superposition of the Ni(II) difference spectrum and that of a transient species. Accordingly, the absorption spectrum of the transient species was obtained by subtracting the TA spectrum acquired at a 50 μs delay, which is well after the system had fully evolved to **2a**, from that acquired at 40 ns. The resulting spectrum displays an absorption maximum at 366 nm as well as a broad band with a maximum at 525 nm; this spectrum of the transient species is shown in Figure 4a. We attribute the observed spectral features to an arene-to-chlorine charge-transfer adduct between a ligand aryl group and a photogenerated chlorine atom. This assignment is based on the similarity of the observed spectral features to those observed for chlorine atom charge-transfer adducts of benzene (Figure S11), generated by either laser flash photolysis or pulse radiolysis.[32−35] The observed spectral features are shifted $\sim$35 nm lower in energy than those in the benzene adduct because of substituent effects (vide infra).[32] The chlorine−benzene complex has been proposed to be an η^1 π complex on the basis of DFT calculations.[36] The assignment is bolstered by examination of the transient species generated by laser-flash photolysis of a derivative of **1a** in which each aryl substituent is
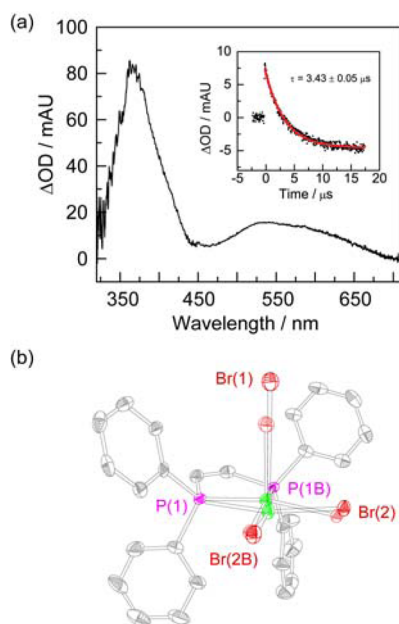
Figure 4. (a) Transient absorption spectrum generated by subtracting the difference spectrum of a 0.44 mM solution of **1a** in CH₃CN acquired at a 50 μs time delay from that acquired at a 40 ns time delay (λ_{exc} = 355 nm). Inset: single-wavelength kinetics trace monitored at 540 nm fit with a monoexponential lifetime of 3.43 ± 0.05 μs (red line). (b) Thermal ellipsoid plot (50% probability) of photocrystallographic analysis of NiBr₃(dppey) **1c**; photoinduced structure (solid; Ni(1)−Br(1) 3.70(4) Å) superimposed on dark structure (faded; Ni(1)−Br(1) 2.464(2) Å). This plot was generated by normalizing the positions of the P centers in the dark and irradiated structures. H atoms and solvent molecules are omitted for clarity.

functionalized with a *para*-methoxy group (4-MeO-**1a**; EPR spectrum in Figure S2). The observed TA line shape is similar to that shown in Figure 4a, but the λ_{max} is red-shifted ∼75 nm compared to that of **1a** (Figure S12). Charge-transfer complexes between arenes and halogen atoms are known to display a linear relationship between the absorption energy and the ionization potential of the donor.[29] We propose that the formation of the relatively long-lived (3.43 μs) transient species (**4**) from a dissociative LMCT excited state (**3**) (vide infra) affords a mechanism to circumvent facile exothermic back reaction of photogenerated Cl radicals with Ni(II) complexes.

Steady-state photocrystallography results are consistent with the photoactivation of the apical halogen bond. As we have previously shown for halogen photoelimination reactions from Rh₂ complexes,[37] atomic displacements during solid-state photoreactions can be directly investigated with X-ray diffraction by comparing diffraction with and without irradiation. Such comparison of these diffraction data sets in a photodifference map can indicate the photoinduced atomic displacements in a crystalline sample. **1c**, NiBr₃(dppey) (dppey = *cis*-bis-(diphenylphosphino)ethylene), was used in these experiments because the bromide ligands have greater electron density as compared to chloride ligands, which makes examination of photoinduced atomic displacement possible at low populations of reaction progress (X-ray structure of **1c** in Figure S13). **1b** was not used in these experiments because of crystallographic disorder in the solid-state structure in the dark. The difference map (Figure 4b), generated from diffraction data collected prior to and during irradiation (λ = 365 nm), shows the presence of a photoinduced structure populated at 3.5(2)% of the crystal

(Figure S14). The photodifference map shows that the apical Ni−Br bond elongates from 2.464(2) to 3.70(4) Å, whereas two basal Ni−Br bonds are crystallographically unchanged (2.3615(7) Å (dark), and 2.35(5) Å (photoinduced)), indicating that the apical halide is photochemically labile. The observed structural changes are neither photochemically nor thermally reversible, consistent with the photoinduced component arising from irreversible Ni−X scission in the solid state. Crystallinity of the samples is destroyed upon further photolysis, also consistent with the operation of a chemically irreversible solid-state reaction. The metrical parameters of **1c** do not exhibit significant temperature dependence, confirming that the photodifference map arises from photochemical, not thermal, M−X activation (Table S3;[38] evaluation of the extent of laser heating on the crystal samples, in Figure S15).

To better understand the ground- and excited-state properties of **1a**, a DFT geometry optimization was performed at the B3LYP level of theory with TZV (C and H) and TZVP (Ni, Cl, and P) basis sets.[39] The ground state is consistent with the delocalized metal-to-apical-ligand bonding description indicated by EPR spectroscopy (e.g., a single unpaired electron in the Ni 3d$_{z^2}$ orbital and spin densities of ∼0.88 and ∼0.17 for Ni(III) and the apical Cl (Cl$_{ap}$), respectively (Table S9)). The β-Mayer bond order (MBO) for the Ni(III)−Cl apical bond is calculated to be ∼0.42. TD-DFT calculations were performed using the optimized geometry of complex **1a**, and the calculated absorption spectrum reproduces the major spectral features observed in the experimental data (Figures 2 (expt) and S16, and Table S10 (calc)). The feature centered ∼620 nm largely consists of apical Cl pσ- and pπ-based transitions to the unoccupied 3d$_{x^2-y^2}$ orbital. The absorption feature in the ∼500−400 nm region largely consists of intense phenyl-ring $\pi \rightarrow$ Ni(3d$_{x^2-y^2}$) charge-transfer transitions and apical/basal Cl(pπ) → Ni-(3d$_{x^2-y^2}$) LMCTs. It is of interest to note that two components in this energy region are predicted to have apical/basal Cl(p(π)) → Ni(3d$_{z^2}$) LMCT character (transitions 4 and 6 in Figure S16 and Table S10 (red lines)). Lastly, an apical Cl(pσ) → Ni(3d$_{z^2}$) LMCT is predicted within the higher-energy absorption envelope (∼360 nm, transition 11, Figure S16 and Table S10), among additional phenyl-ring $\pi \rightarrow$ Ni(3d$_{x^2-y^2}$) LMCTs. These assignments are consistent with the persistence of higher-energy absorption features and the complete disappearance of the lower-energy feature upon photoreduction of **1** to form **2**. Interestingly, LMCT to the unoccupied p$_z$/d$_{z^2}$ antibonding Ni-based hole (e.g., the β-LUMO) leads to the formal elimination of any apical Ni−Cl bond order (Figures S17 and S18). Therefore, excited states with LMCT character to the β-LUMO may be responsible for the photoinduced cleavage of the apical Ni(III)−Cl bond.[40]

Scheme 1 illustrates a halogen extrusion mechanism that is consistent with the spectroscopic, photochemical, photocrystallographic, and computational experiments. Photon absorption by **1** provides access to **3**. Steady-state photocrystallography experiments indicate that the apical halide, which displays a substantially longer M−X bond than the basal halide ligands, is selectively eliminated. Participation of ligand-based aromatic substituents via **4** stabilizes the photodissociated chlorine atom in the secondary coordination sphere of the metal complex. Intermediate **4** displays a microsecond lifetime, which we propose serves to provide sufficient time to assist the removal of halogen from the primary coordination sphere, thereby leading to productive elimination chemistry by circumventing the exothermic back reaction. In solution-phase experiments, the photodissociated chlorine atom is likely

Scheme 1. Proposed Photoreduction of Complex 1a Proceeds via an LMCT Excited State (3) to Furnish the Arene-to-Cl Charge-Transfer Intermediate 4
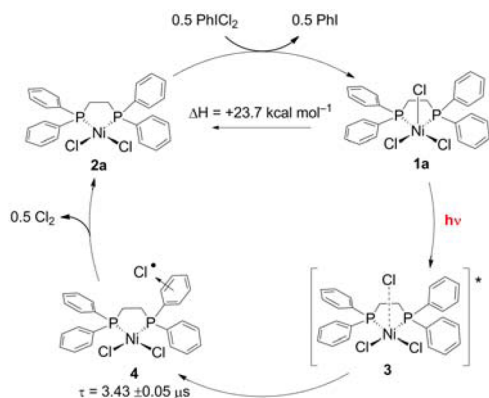
intercepted by solvent via H atom abstraction,[24−26] whereas in the solid state in the absence of chemical traps, dimerization affords Cl_2.

Authentic halogen photoelimination from mononuclear Ni(III) complexes has been achieved with visible light. The photoreaction is substantially endothermic; calorimetry experiments have established chlorine elimination stores 23.7 kcal mol^{-1}. Relatively long-lived chlorine atom adducts are observed, and they are on-pathway for photochemical elimination. The interaction of the eliminated chlorine atom with the aromatic moieties in the second coordination sphere provides a mechanism to achieve halogen elimination in preference to the back reaction of evolved Cl_2 with Ni(II) photoproducts and offers an attractive design strategy to realize productive energy-storing photochemistry from 3d transition-metal complexes.

ASSOCIATED CONTENT

Ⓢ Supporting Information

Detailed experimental procedures, spectroscopic data, XYZ coordinates of computed structures, and the full ref 39. The Supporting Information is available free of charge on the ACS Publications website at DOI: 10.1021/jacs.5b03192.

AUTHOR INFORMATION

Corresponding Author
*dnocera@fas.harvard.edu

Notes
The authors declare no competing financial interest.

ACKNOWLEDGMENTS

REFERENCES

(1) Esswein, A. J.; Nocera, D. G. *Chem. Rev.* **2007**, *107*, 4022.
(2) Nocera, D. G. *Inorg. Chem.* **2009**, *48*, 10001.
(3) Teets, T. S.; Nocera, D. G. *Chem. Commun.* **2011**, *47*, 9268.
(4) Cook, T. R.; Surendranath, Y.; Nocera, D. G. *J. Am. Chem. Soc.* **2009**, *131*, 28.
(5) Lin, T.-P.; Gabbaï, F. P. *J. Am. Chem. Soc.* **2012**, *134*, 12230.
(6) Yang, H.; Gabbaï, F. P. *J. Am. Chem. Soc.* **2014**, *136*, 10866.
(7) Karikachery, A. R.; Lee, H. B.; Masjedi, M.; Ross, A.; Moody, M. A.; Cai, X.; Chui, M.; Hoff, C. D.; Sharp, P. R. *Inorg. Chem.* **2013**, *52*, 4113.
(8) Perera, T. A.; Masjedi, M.; Sharp, P. R. *Inorg. Chem.* **2014**, *53*, 7608.
(9) Teets, T. S.; Nocera, D. G. *J. Am. Chem. Soc.* **2009**, *131*, 7411.
(10) Powers, D. C.; Chambers, M. B.; Teets, T. S.; Elgrishi, N.; Anderson, B. L.; Nocera, D. G. *Chem. Sci.* **2013**, *4*, 2880.
(11) Cook, T. R.; Esswein, A. J.; Nocera, D. G. *J. Am. Chem. Soc.* **2007**, *129*, 10094.
(12) Cook, T. R.; McCarthy, B. D.; Lutterman, D. A.; Nocera, D. G. *Inorg. Chem.* **2012**, *51*, 5152.
(13) Teets, T. S.; Lutterman, D. A.; Nocera, D. G. *Inorg. Chem.* **2010**, *49*, 3035.
(14) For a recent exception, see Powers, D. C.; Hwang, S. J.; Zheng, S.-L.; Nocera, D. G. *Inorg. Chem.* **2014**, *53*, 9122.
(15) Du, J.; Chen, Z.; Chen, C.; Meyer, T. J. *J. Am. Chem. Soc.* **2015**, *137*, 3193.
(16) Creutz, C.; Chou, M.; Netzel, T. L.; Okumura, M.; Sutin, N. *J. Am. Chem. Soc.* **1980**, *102*, 1309.
(17) McCusker, J. K. *Acc. Chem. Res.* **2003**, *36*, 876.
(18) Juban, E. A.; Smeigh, A. L.; Monat, J. E.; McCusker, J. K. *Coord. Chem. Rev.* **2006**, *250*, 1783.
(19) Powers, D. C.; Anderson, B. L.; Nocera, D. G. *J. Am. Chem. Soc.* **2013**, *135*, 18876.
(20) Hwang, S. J.; Powers, D. C.; Maher, A. G.; Nocera, D. G. *Chem. Sci.* **2015**, *6*, 917.
(21) Fredin, L. A.; Pápai, M.; Rozsályi, E.; Vankó, G.; Wärnmark, K.; Sundström, V.; Persson, P. *J. Phys. Chem. Lett.* **2014**, *5*, 2066.
(22) Gray, L. R.; Higgins, S. J.; Levason, W.; Webster, M. *J. Chem. Soc., Dalton Trans.* **1984**, 459.
(23) Bruin, B. D.; Hetterscheid, D. G. H.; Koekkoek, A. J. J.; Grützmacher, H. In *Prog. Inorg. Chem.*; Karlin, K. D., Ed.; J. Wiley and Sons: New York, 2007; Vol. *55*, p 247.
(24) Kurylo, M. J.; Knable, G. L. *J. Phys. Chem.* **1984**, *88*, 3305.
(25) Tyndall, G. S.; Orlando, J. J.; Wallington, T. J.; Sehested, J.; Nielsen, O. J. *J. Phys. Chem.* **1996**, *100*, 660.
(26) Sheps, L.; Crowther, A. C.; Elles, C. G.; Crim, F. F. *J. Phys. Chem. A* **2005**, *109*, 4296.
(27) Kasha, M. *Discuss. Faraday Soc.* **1950**, *9*, 14.
(28) Lide, D. R. *CRC Handbook of Chemistry and Physics*, 85th ed.; CRC Press: Boca Raton, FL, 2004; pp 1−15.
(29) Nickel, U.; Chen, Y.-H.; Schenider, S.; Silva, M. I.; Burrows, H. D.; Formosinho, S. J. *J. Phys. Chem.* **1994**, *98*, 2883.
(30) Bader, H.; Sturzenegger, V.; Hoigné, J. *Water Res.* **1988**, *22*, 1109.
(31) Andrews, L. J.; Keefer, R. M. *J. Am. Chem. Soc.* **1958**, *80*, 1723.
(32) Bühler, R. E.; Ebert, M. *Nature* **1967**, *214*, 1220.
(33) Strong, R. L.; Rand, S. J.; Britt, J. A. *J. Am. Chem. Soc.* **1960**, *82*, 5053.
(34) Bossy, J. M.; Bühler, R. E.; Ebert, M. *J. Am. Chem. Soc.* **1970**, *92*, 1099.
(35) Förgeteg, S.; Bérces, T. *J. Photochem. Photobiol., A* **1993**, *73*, 187.
(36) Tsao, M.-L.; Hadad, C. M.; Platz, M. S. *J. Am. Chem. Soc.* **2003**, *125*, 8390.
(37) Powers, D. C.; Anderson, B. L.; Hwang, S. J.; Powers, T. M.; Pérez, L. M.; Hall, M. B.; Zheng, S.-L.; Chen, Y.-S.; Nocera, D. G. *J. Am. Chem. Soc.* **2014**, *136*, 15346.
(38) Schmøkel, M. S.; Kamiński, R.; Benedict, J. B.; Coppens, P. *Acta Crystallogr., Sect. A* **2010**, *66*, 632.
(39) Frisch, M. J.; Trucks, G. W.; Schlegel, H. B.; Scuseria, G. E.; Robb, M. A.; Cheeseman, J. R.; Scalmani, G.; Barone, V.; Mennucci, B.; Petersson, G. A.; et al. *Gaussian 09*, revision D.01; Gaussian, Inc.: Wallingford, CT, 2009.
(40) Sokolov, A. Y.; Schaefer, H. F., III *Dalton Trans.* **2011**, *40*, 7571.